Nucl. Fusion **49** (2009) 104013 (9pp) doi:10.1088/0029-5515/49/10/104013

Overview of the FTU results

A.A. Tuccillo[1], A. Alekseyev[2], B. Angelini[1], S.V. Annibaldi[3], M.L. Apicella[1], G. Apruzzese[1], J. Berrino[4], E. Barbato[1], A. Bertocchi[1], A. Biancalani[5], W. Bin[4], A. Botrugno[1], G. Bracco[1], S. Briguglio[1], A. Bruschi[4], P. Buratti[1], G. Calabrò[1], A. Cardinali[1], C. Castaldo[1], C. Centioli[1], R. Cesario[1], L. Chen[6], S. Cirant[4], V. Cocilovo[1], F. Crisanti[1], R. De Angelis[1], U. de Angelis[7], L. Di Matteo[1], C. Di Troia[1], B. Esposito[1], G. Fogaccia[1], D. Frigione[1], L. Gabellieri[1], F. Gandini[4], E. Giovannozzi[1], G. Granucci[4], F. Gravanti[1], G. Grossetti[4], G. Grosso[4], F. Iannone[1], H. Kroegler[1], V. Lazarev[2], E. Lazzaro[4], I.E. Lyublinski[8], G. Maddaluno[1], M. Marinucci[1], D. Marocco [1], J.R. Martin-Solis[9], G. Mazzitelli[1], C. Mazzotta[1], V. Mellera[4], F. Mirizzi[1], S. Mirnov[2], G. Monari[1], A. Moro[4], V. Muzzini[4], S. Nowak[4], F.P. Orsitto[1], L. Panaccione[1], D. Pacella[1], M. Panella[1], F. Pegoraro[5], V. Pericoli-Ridolfini[1], S. Podda[1], S. Ratynskaia[3], G. Ravera[1], A. Romano[1], A. Rufoloni[1], A. Simonetto[4], P. Smeulders[1], C. Sozzi[4], E. Sternini[1], B. Tilia[1], O. Tudisco[1], A. Vertkov[8], V. Vitale[1], G. Vlad[1], R. Zagórski[10], M. Zerbini[1] and F. Zonca[1]

[1] Associazione Euratom-ENEA sulla Fusione, Via E. Fermi 45, 00044 Frascati, Roma, Italy
[2] TRINITI, Troitsk, Moscow Reg., Russia
[3] Association Euratom-VR, Royal Institute of Technology, SE-10044 Stockholm, Sweden
[4] Associazione EURATOM-ENEA, IFP-CNR, Via R. Cozzi, 53 20125 Milano, Italy
[5] Physics Department, University of Pisa, 56127 Pisa, Italy
[6] Department of Physics and Astronomy, University of California, Irvine, CA 92697-4575, USA and Institute for Fusion Theory and Simulation, Zhejiang University, Hangzhou, People's Republic of China
[7] Dipartimento di Fisica,Universita di Napoli and INFN Sezione di Napoli, Italy
[8] FSUE 'Red Star', Electrolitnij Proezd, 1a, Moscow, 115230, Russian Federation
[9] Departamento de Fısica, Universidad Carlos III De Madrid, 28911 Leganes, Madrid, Spain
[10] Institute of Plasma Physics and Laser Microfusion, EURATOM Association, 01-497, Warsaw, PL

E-mail: tuccillo@frascati.enea.it

Received 29 January 2009, accepted for publication 17 March 2009
Published 9 September 2009
Online at stacks.iop.org/NF/49/104013

Abstract
Spontaneous increases in plasma density, up to ∼1.6 times the Greenwald value, are observed in FTU with lithized walls. These plasmas are characterized by profile peaking up to the highest obtained densities. The transport analysis of these discharges shows a 20% enhancement of the energy confinement time, with respect to the ITER97 L-mode scaling, correlated with a threshold in the peaking factor. It has been found that 0.4 MW of ECRH power, coupled at $q = 2$ surface, are sufficient to avoid disruptions in 0.5 MA discharges. Direct heating of magnetic islands produced by MHD modes determines current quench delay or avoidance. Supra-thermal electrons generated by 0.5 MW of lower hybrid power are sufficient to trigger precursors of the electron-fishbone instability. Evidence of spatial redistribution of fast electrons, on the ∼100 μs typical mode timescale, is shown by the fast electrons bremsstrahlung diagnostic. From the presence of new magnetic island induced accumulation points in the continuous spectrum of the shear Alfvén wave spectrum, the existence of new magnetic island induced Alfvén eigenmodes (MiAE) is suggested. Due to the frequency dependence on the magnetic island size, the feasibility of utilizing MiAE continuum effects as a novel magnetic island diagnostic is also discussed. Langmuir probes have been used on FTU to identify hypervelocity (10 km s^{-1}), micrometre size, dust grains. The Thomson scattering diagnostic was also used to characterize the dust grains, present in the FTU vacuum chamber, following a disruption. Analysis of the broad emitted light spectrum was carried out and a model taking into account the particle vaporization is compared with the data. A new oblique ECE diagnostic has been installed and the first results, both in the presence of lower hybrid or electron cyclotron waves, are being compared with code predictions. A time-of-flight refractometer at 60 GHz, which could be a good candidate for the ITER density feedback control system, has also been tested.

PACS numbers: 52.55.Fa, 52.25.Fi, 52.50.Sw, 52.35.Bj, 52.27.Lw

(Some figures in this article are in colour only in the electronic version)

1. Introduction

In the last two years, FTU [1] has continued its experimental programme in support of ITER physics providing plasma scenarios and operations at ITER-relevant density and magnetic field as well as exploiting liquid lithium as plasma facing material. Moreover, the combination of FTU heating systems, electron cyclotron resonant heating (ECRH, 140 GHz) and lower hybrid (LH, 8 GHz) [1], provides plasma scenarios with direct electron heating and current drive without momentum input as expected in ITER. In shaping the FTU scientific programme of the last two years, the emphasis has been put on emerging research themes such as electron-fishbone [2, 3], which allows addressing aspects of burning plasma non linear dynamics already in the present day machines, and on optimizing operations with the liquid lithium limiter (LLL) to demonstrate its capability as plasma facing component (PFC) under harsh conditions [4]. Disruption avoidance has been obtained through off-axis deposition of ECRH triggered just before the quench of induced plasma disruptions. A detailed calculation of the ECRH power deposition has allowed a better understanding of the MHD behaviour, ultimately responsible for the disruption [5], and provided preliminary information on the power threshold for disruption avoidance. A strong synergy on this activity is coming from the collaboration between IPP and CRPP laboratories, allowing the comparison of similar stabilizing schemes in very different plasma configurations. The well-established collaboration between the FTU group, the University of Pisa and the University of California at Irvine has continued on the study of shear Alfvén waves (SAWs) nonlinear behaviours, involving close connection and synergy between theory and experiments. Here, new structures in the low-frequency SAW continuous spectrum have been shown to exist, due to finite size magnetic islands, and the existence of new MiAE is suggested, when radially localized bound stated are excited within these structures. Preliminary analyses of FTU observations of beta induced Alfvén eigenmodes in the presence of finite size magnetic islands [6–8] show frequency dependences on the island width, which are consistent with the theoretical scaling of the MiAE continuum accumulation point [9]. Last but not least, some experimental time has been devoted to studying the formation and dynamics of metallic dust. In fact, hypervelocity ($10\,\mathrm{km\,s^{-1}}$), micrometre size, dust grains have been detected. Characterization of the grains has been attempted by means of a Thomson scattering diagnostic [10], analysing the light scattered by the grains produced after disruptions. Other relevant themes of the FTU programme, as the study of advanced tokamak scenarios, have been put at a lower priority due to the ongoing refurbishment of heating systems. With full LH and ECRH power, advanced tokamak scenarios will be addressed again at higher current and density, thus in conditions of efficient electron–ion coupling. In this paper, the results of the last two years will be overviewed: the study of high density discharges obtained with LLL will be reported in the next section, while section 3 focuses on experimental and theoretical studies of electron fishbones and SAW. Section 4 provides highlights of the results on disruption mitigation with ECRH, while section 5 summarizes those on dust. Finally, in section 6 some preliminary results on minor diagnostics upgrade will be reported, together with the planning of the near future activity on FTU while some conclusions are drawn in section 7.

2. Improved performance in high density discharges with lithized walls

In a reactor relevant environment, where heat loads can exceed $20\,\mathrm{MW\,m^{-2}}$, it would be of great advantage to use a liquid plasma-limiting material. This could flow in an adequate structure, thus compensating for the erosion losses due to evaporation, splashing and ion sputtering, provided that the containing structure would effectively contain the liquid under harsh conditions it should withstand. Since 2005, a LLL [11] based on the capillary porous system [12] has been installed on FTU. It is located in the bottom part of the vacuum chamber, resting in the shadow of the inner side toroidal limiter. When required by the programme it can be moved and can act as an effective plasma facing limiter. The LLL experiment on FTU aims at studying plasma performance in the presence of lithized walls as well as at testing the capillary porous system capability to contain liquid lithium in the presence of the heavy heat loads produced in FTU. Since its installation, FTU operations have the benefit of faster restarts after shutdowns, easy access to high density, up to 1.6 times the Greenwald's limit and clean operations with $Z_{\mathrm{Eff}} \sim 1$ in a wide range of densities [13]. Interestingly, strongly peaked density profiles are obtained up to the highest density values, resembling, for many aspects, those obtained in pellet-fuelled discharges [4]. In lithized discharges, intrinsic metallic impurities (Mo, Fe, Ni) are strongly reduced ($Z_{\mathrm{Eff}} \sim 1$), while an increase of the SOL temperature, with respect to that measured in ordinary not-lithized ohmic discharges is measured by the Langmuir probes, both at $I_{\mathrm{P}} = 0.5\,\mathrm{MA}$ and $I_{\mathrm{P}} = 0.75\,\mathrm{MA}$ [14]. A large database of ohmic discharges, obtained with the new LLL facility, demonstrates peculiar aspects of enhanced confinement behaviour. A detailed transport analysis of the new scenario has been performed: focusing in particular on the comparison with results of analogous studies on the bulk of ohmic 'pre-lithium' FTU discharges [15].

The analysed database contains discharges with: $\bar{n}_{\mathrm{e}} = (0.6\text{–}2.8) \times 10^{20}\,\mathrm{m^{-3}}$, $I_{\mathrm{P}} = 0.5\,\mathrm{MA}$, $B_{\mathrm{T}} = 6\,\mathrm{T}$ and few discharges at higher plasma current (0.7–0.75 MA). Transport analyses have been performed with the JETTO code [16], taking as input the Z_{eff} evolution from visible bremsstrahlung signals and the electron temperature and density profiles, as they respectively result from Thomson scattering and CO_2 interferometer diagnostics. The ion temperature profile is derived by assuming a neoclassical transport model with an 'anomalous' multiplicative coefficient calibrated by the constraint of matching the experimental neutron rate. The radiation power density profile has been deduced from bolometer taking into account the data obtained by spectroscopy on impurities concentrations, mainly consisting of lithium and a small fraction of oxygen. In all the analysed discharges, ion transport is neoclassical with an anomaly coefficient close to 1. As can be seen in figure 1, where the time evolution of two high (and peaked profile) density discharges ($\bar{n}_{\mathrm{e}} = (2.7\text{–}2.8) \times 10^{20}\,\mathrm{m^{-3}}$) is shown, a sharp transition from a low to a higher energy confinement

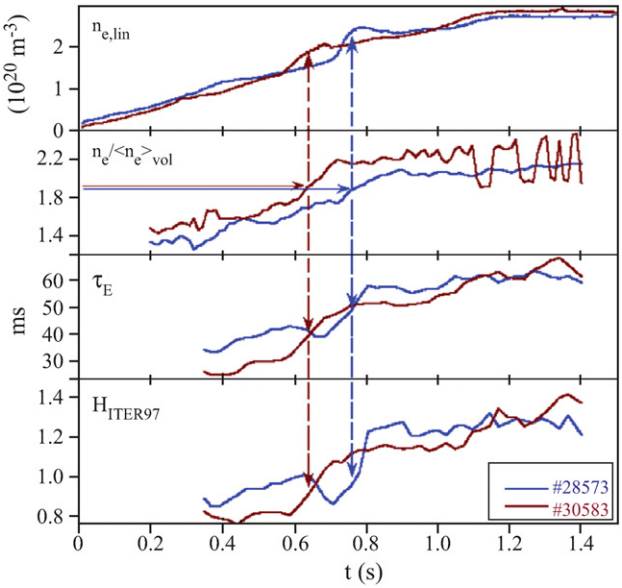

Figure 1. Time evolution of line averaged density, peaking factor, energy confinement time and H_{97} in two high-density discharges. In both cases, the transition to higher τ_E occurs at the same value of $n_{e0}/\langle n_e\rangle_{vol}$.

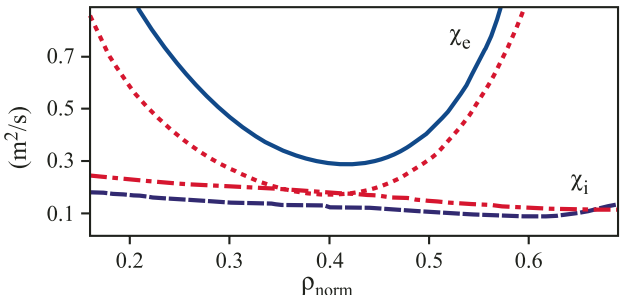

Figure 2. Electron and ion thermal conductivity for shot #28573 before and after the increase in the volume density peaking factor. Electrons: continuous line before density peaking, dotted line after; ions: dashed line before, dashed-dotted line after.

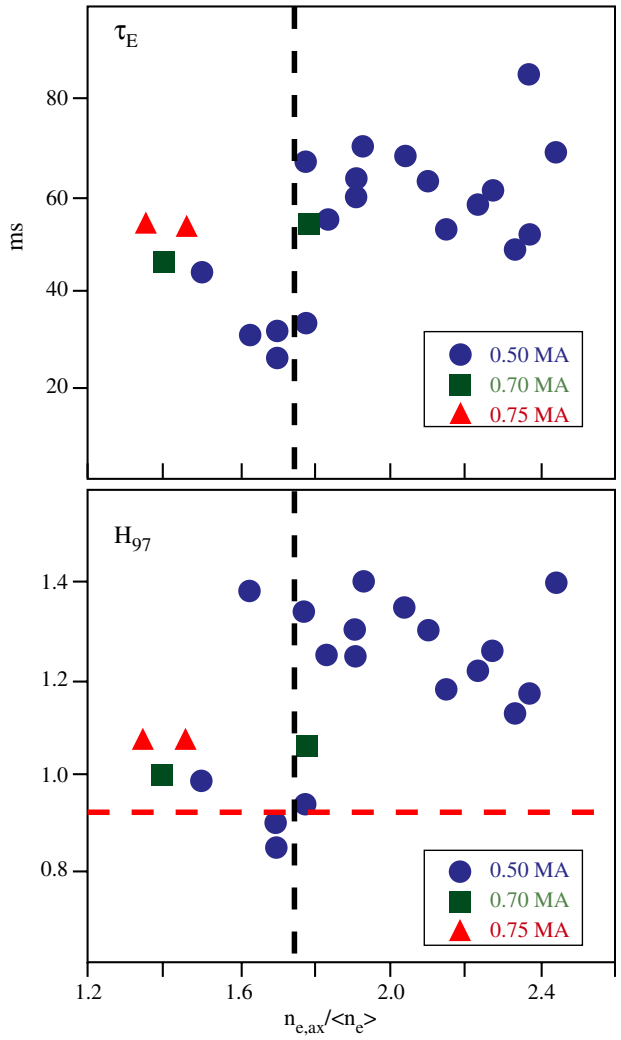

Figure 3. τ_E (Top) and H_{97} (Bottom) versus volume density peaking factor in 'lithized' discharges.

regime occurs around 0.6 and 0.8 s. In both discharges, the transition seems to occur as soon as the density profile begins effectively to peak at the same threshold value of 1.75–1.8. The improved confinement results in an enhancement of the ITER-97 L-mode scaling (H_{97}), which rises from $H_{97} \cong 0.92$ to $H_{97} \cong 1.25$.

The electron and ion thermal conductivities (χ_e and χ_i) are shown in figure 2 before and after the transition to the enhanced confinement phase. In the peaked, high-density phase, χ_e is about a factor 2 lower than in the not-peaked phase and it takes the value of $\sim 0.2\ m^2\ s^{-1}$, which is typical of the saturated ohmic confinement (SOC) regime [15]. However, in the peaked density phase heat transport keeps being dominated by electron conductivity, while ion conductivity remains close to its neoclassical value. From the analysis of the whole database of lithized discharges, the existence of the density peaking factor threshold, at which the improved confinement regime appears, seems confirmed. The results of this analysis are reported in figure 3, where the energy confinement time τ_E and the enhancement on the ITER97-L scaling H_{97} are shown versus the volume density peaking factor ($n_{e0}/\langle n_e\rangle$).

The presence of a second regime of better confinement, up to a factor 1.4 above $\tau_{ITER97\text{-}L}$, come out clearly as a general behaviour of the lithized discharges, at least at $I_p = 0.5$ MA. The few analysed cases at 0.7 and 0.75 MA are also reported in the figure, but more data are needed to conclude whether an analogous transition also occurs at higher currents. It is important to note that, regardless of the density value, almost all the lithized-wall discharges tend to have peaked density profiles above the threshold value [17]. Analyses of turbulence behaviour and stability properties are in progress to assess the origin of the transition above the density peaking threshold.

A comparison between τ_E of the 'lithized' discharges with that of the 'pre-lithium' FTU ohmic discharges in the SOC phase, both gas-fuelled and pellet-fuelled, shows that the presence of lithized walls produces a rise in the saturated confinement threshold value from about 45–50 ms to about 65–70 ms. As in the case of pellet-fuelled discharges, discussed in [5, 17], this behaviour is accompanied by a sharp increase in the peaking of the density profile and by neoclassical ion transport.

3. Theory and modelling of experimental observations

3.1. Electron-fishbones in FTU plasmas

The interaction of trapped alpha particles with low-frequency MHD modes in burning plasmas is characterized by a small $\rho_* = \rho_L/a$, i.e. the ratio of particle Larmor radius to the machine size. That trapped particle bounce-averaged dynamics depends on energy and not on mass, together with the small ρ_*, makes trapped fusion alphas behaviour similar to that of trapped supra-thermal electron in present day experiments [2]. Consequently, the fishbone-like internal kink instability driven by supra-thermal electrons generated by LHCD or ECRH and, more generally, fast electron driven MHD modes are of great interest for addressing burning plasmas issues. Fishbone-like internal kink instabilities driven by fast electrons were observed during FTU experiments aimed at producing internal transport barriers with LHCD, used to optimize the q-profile evolution [18].

Theoretical analyses [2] interpreted this quasi-stationary fluctuation as a 'fixed point' solution of the nonlinear dynamical system, produced by supra-thermal electrons in the presence of a moderately hollow q-profile with $q_{\min} \sim 1$, undergoing a transition to 'limit cycle' bursting behaviour as LH power is increased. A similar instability was previously observed on DIII-D during high-field-side ECRH experiments and attributed to excitations by barely trapped supra-thermal electrons, characterized by drift reversal [19].

More recently in Tore Supra, the data of the hard-x-ray diagnostic (60–80 keV) provided clear indication of spatial redistribution of the supra-thermal electron population [20]. However, the time behaviour of this phenomenon, with respect to the MHD timescale (0.1 ms), could not be followed in detail due to the insufficient time resolution of the diagnostic (16 ms). On FTU, the fast electron bremsstrahlung (FEB) camera is equipped with a very fast digitizer system that records the single photon event allowing any type of sophisticated data analysis. Besides data statics, the time resolution of the diagnostics is only limited by the pulse shaping, resulting in a minimum 4 μs [3]. An experimental campaign has started on FTU to systematically assess the short timescale and possibly bursting behaviour of electron-fishbone as foreseen by the theoretical model [2]. Optimal plasma conditions are provided by lithized walls [4] (low Z_{eff} and good SOL conditions for LH) and by an accurate choice of the LHCD power waveforms, which guarantees a robust control of q-profile evolution [21]. Recent experiments on FTU show that electron-fishbone activity, with 'fixed point' oscillations behaviour, already appears with as low as 0.5 MW of LH power. The power is applied at the end of the ramp-up phase of an $I_P = 0.5$ MA discharge. For the duration of the LH pulse, the q profile remains constant and is characterized by a flat central region with $q_0 \leqslant 1$. At the switch off of LH power, the electron-fishbone activity disappears and only sawteeth survive. Detailed analyses of MHD data provided by soft x-ray tomography [22], and of data recorded by the FEB camera, have allowed the reconstruction of the hard x-ray emission profile on the fishbone timescale ($\sim$0.1 ms). Preliminary results are shown in figure 4. Here, fast electrons profiles are shown as obtained inverting FEB data and integrating them in phase over ten fishbone oscillations to improve the statistic. Comparing the profile obtained in the half positive part of the mode oscillation with that obtained in the half negative part a spatial redistribution of the fast electrons, associated with the kink structure of the mode, can be inferred during typical quasi-stationary oscillations. The redistribution appears to be localized close to the radial position of mode and to occur on the same time scale. The differences between profiles are well above the error bar thanks to statistic improvements due to data integration phased with the mode oscillation [3]. In figure 5 the profiles obtained integrating the FEB data in a 3 ms window, sliding along the fishbone activity, are reported. Here more realistic information can be inferred about the influence of the mode on the effective fast electron transport. Spatial redistribution seems to occur across layers centred at $r/a \approx 0.3$. The evolution of the profile at minor normalized radius $r/a = 0.25$, where the LH deposition is centred, is in agreement with the quasi-linear time [23], $t \approx 2.8$ ms, estimated for the discharge analysed and a LH power of 0.5 MW. By comparing energy spectra in time windows centered at the beginning of the fluctuations cycle and after the peak intensity of the mode, respectively, the electron-fishbone induced profile broadening is seen for resonant supra-thermal electrons with energies in the range 60 keV $\leqslant E \leqslant$ 100 keV [2].

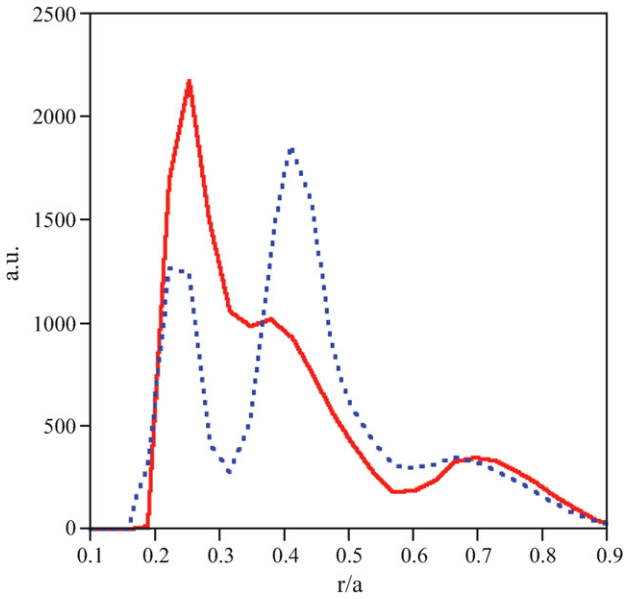

Figure 4. Fast electron radial profiles by inverted FEB camera data. Profiles are obtained integrating in phase ten fishbone oscillation periods: during positive half period (continuous curve) and during negative half period (dotted curve). Energy range 40–60 keV.

3.2. SAW continuous spectrum in the presence of a magnetic island

In fusion plasmas, fast ions in the MeV energy range have velocities comparable to the typical Alfvén speed and can therefore resonantly interact with SAW. On the other end SAW in non-uniform equilibrium experience energy absorption (continuum damping [24]), due to singular structures that are formed at the SAW continuum resonant surfaces. Because of

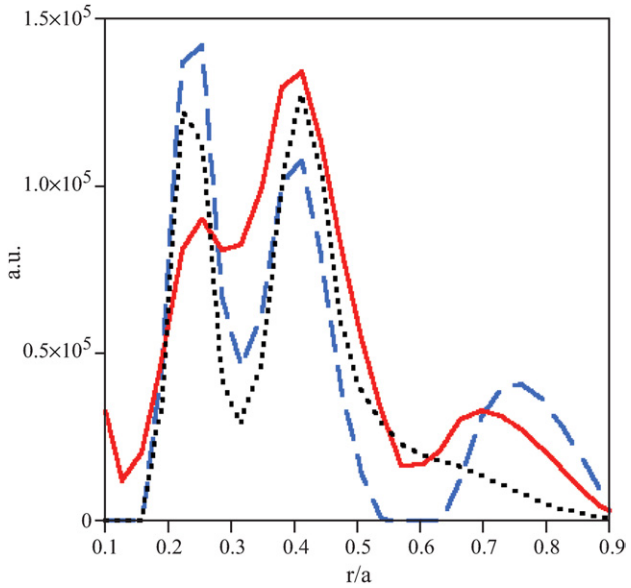

Figure 5. Fast electron radial profiles by inverted FEB camera data. Profiles are obtained with 3 ms integration window sliding across the mode: before the maximum of the mode (dashed line), after the maximum (full line) and at the end of the mode (dotted line). Energy range 40–60 keV.

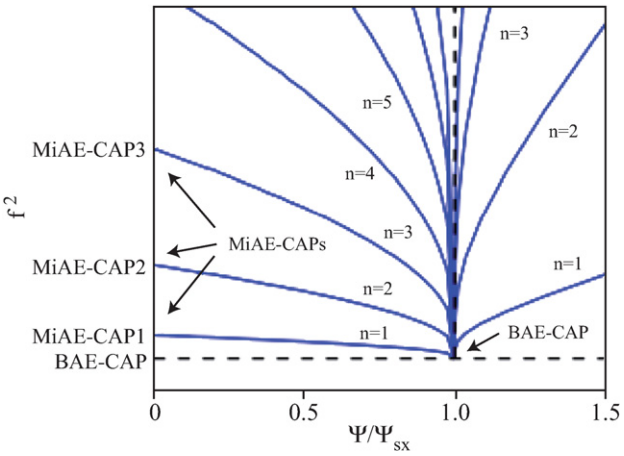

Figure 6. SAW continuous spectrum for various n-modes. The BAE-CAP is shown at the separatrix ($\psi = \psi_{sx}$ where ψ is magnetic flux surface variable) with the new MiAE accumulation points at the O-point ($\psi = 0$).

non-uniformities along the magnetic field lines, gaps appear in the SAW continuous spectrum [25], forming regions free of continuum damping [25]. For this reason, the importance of understanding SAW continuous spectrum structure is clear when analysing SAW stability in tokamaks and its potential impact on the fusion performance. The SAW continuous spectrum can be modified by the interaction with low-frequency MHD fluctuations, such as magnetic islands [26].

We derive our fluid theoretical description of the SAW continuum structure in finite-beta plasmas in presence of a finite size magnetic island [27], keeping into account geodesic curvature effects, which are responsible for beta induced Alfvén eigenmodes (BAE) gap in the low-frequency SAW continuous spectrum [28]. The BAE continuum accumulation point (BAE-CAP) is shifted in space from the island rational surface, $\psi = 0$, to the separatrix flux surface position, $\psi = \psi_{sx}$, while the frequency f_{BAE} remains the same. Here, ψ is the magnetic flux coordinate. New magnetic island induced CAPs (MiAE-CAPs) are found at the O-point of the island and, consequently, new gaps exist in the SAW continuous spectrum (see figure 6). This result has potential implications in the analysis of stability properties of tokamak plasmas in the presence of magnetic islands. In fact, new MiAE could be excited within a magnetic island if the thermal or energetic components of the plasma provide sufficient free energy for driving the mode. Modes in the BAE frequency range have been observed in FTU [6], in the presence of an $(m, n) = (-2, -1)$ magnetic island, m/n indicating poloidal/toroidal mode numbers. A theoretical analysis has shown that these modes can be interpreted as BAE modes, when thermal ion transit resonances and finite ion Larmor radius effects are accounted for [7], with good agreement of measured and calculated frequencies in the small magnetic island amplitude limit. In fact, their measured frequency has been found to depend on the island amplitude as well. Similar observations have been reported by TEXTOR [8]. Figure 7 shows the dependence of experimental frequency of modes seen in FTU on the magnetic island fluctuating field. This dependence is consistent with the MiAE-CAP scaling [9]. The magnetic island fluctuating field at the rational surface has been reconstructed from that at the Mirnov coil position. Due to the dependence of the MiAE-CAP frequency on mode numbers and magnetic island size, the possibility of using this scaling as novel magnetic island diagnostic is an attractive option. Information on the radial structure of the new MiAE with respect to the more conventional BAE-like gap-modes is given on the basis of mode couplings with the SAW continuum structures shown in figure 6 and their consequences on radial mode localization. If BAEs can extend over a radial range not limited by the island size, on the contrary MiAEs are very localized and positioned at the island centre. Thus, MiAEs cannot be easily detected by diagnostic systems, which measure fluctuating fields at the plasma boundary, such as Mirnov coils. However, we could observe these modes with ECE or soft x-rays diagnostics. The fact that observed mode frequencies are lower than that of the BAE-CAP, $f_{BAE\text{-}CAP} = 60$ kHz ($T_e = T_i = 0.5$ keV, $R = 93.5$ cm), confirms the interpretation of these fluctuations as BAE nonlinearly interacting with the magnetic island [7].

4. ECRH power acting to control plasma disruptions

Control of disruptions is one of the most challenging issues for ITER operations and a key milestone to be achieved on the path to the reactor.

It can be expected, as shown in JET experiments [29], that high performance plasmas revert to the L-mode regime in the pre-disruption phase, with the exception of disruptions induced by vertical displacement. Developing disruption control techniques in small experiments, with L-mode plasmas, would then be directly relevant for ITER and future reactors-grade machines. Presently 'massive gas injection' seems to be the most likely candidate for disruption control in ITER, although the use of ECRH represents an excellent alternative. Recent experiments on FTU [5, 30], as well as on ASDEX

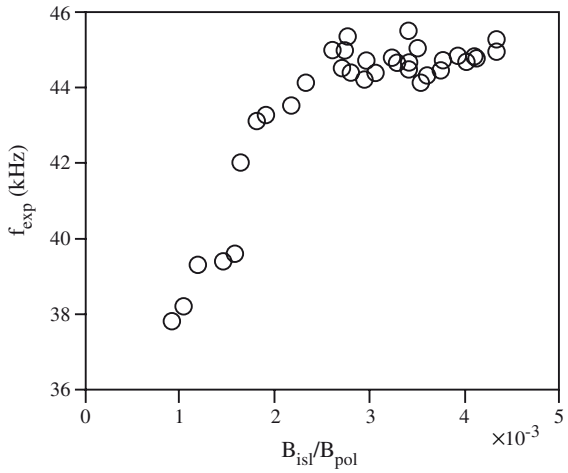

Figure 7. Mode frequency versus magnetic island amplitude observed in FTU shot 25877.

Upgrade [5, 31], indicate how the application of ECRH at specific radial locations can prevent or postpone the disruption.

Disruptions are induced on FTU by injecting Mo into the plasma via laser blow-off, and only in a few cases by puffing deuterium above the Greenwald limit. In the latter case the discharges are limited at 0.35 MA to avoid the 140 GHz ECRH density cut-off, $n_{\text{e-cutoff}} \sim 2.4 \times 10^{20}\,\text{m}^{-3}$. Disruptions control is then studied by triggering ECRH power at a pre-selected loop voltage level (about twice the level in steady state the phase) with pulse duration normally of 100 ms. The magnetic field is kept constant ($B_T = 5.3$ T) while the ECRH launching mirrors are steered, before every discharge, to inject the power at different plasma locations. A comparison of two discharges with and without ECRH is shown in figure 8. Typically, the modes grow up, quickly slow down and then lock. The application of ECRH modifies the starting time of the current quench according to power deposition location (r_{dep}). Disruption avoidance and complete discharge recovery is obtained when P_{ECRH} is applied on rational surfaces, whereas the current quench is progressively delayed when the r_{dep} is approaching a rational surface from the outer side. The analysis of Mirnov coils, fast ECE and soft x-ray tomography shows that $m/n = 3/2$, 2/1, 3/1 modes are generally present with the 2/1 having the largest amplitude. Direct heating, above a threshold value, of one of the magnetic islands prevents its further growth and produces the stabilization of the other coupled MHD modes avoiding or delaying the current quench as summarized in figure 9.

Injected P_{ECRH} has been varied in the range 0.4–1.2 MW and the absorbed fraction has been evaluated by the ECWGB 3D code [32]. An ECRH power of 0.4 MW, deposited at the $q = 2$ surface, is sufficient to avoid disruptions in 0.5 MA discharges while in a 0.35 MA discharge 0.8 MW are needed. The Rutherford equation [33] has been used to reproduce the evolution of the MHD modes that are found to be conventional tearing modes stabilized by a strong local ECRH heating. The results of the simulation for discharge 29479 are compared with the experimental data in figure 10.

The mode coupling effects resulting from the FTU r_{dep} scans are interesting in view of a possible application of such a ECRH control technique to ITER. Various schemes can be

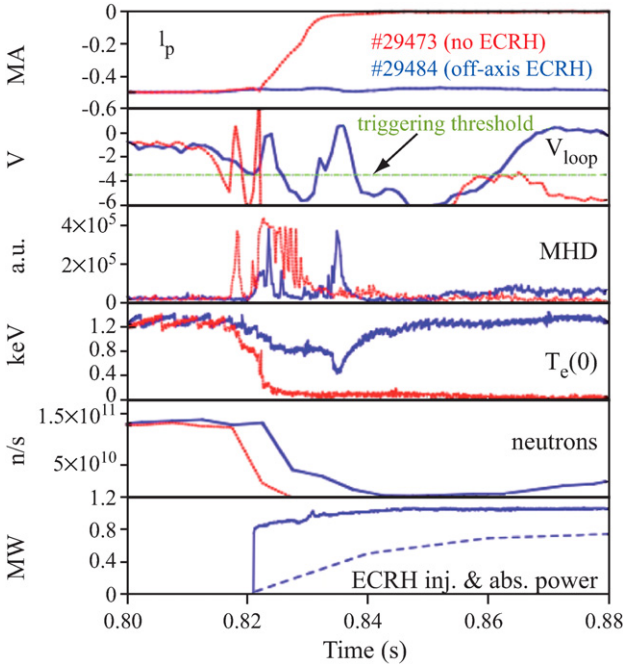

Figure 8. Comparison between two FTU discharges with/without ECRH. The disruption is avoided in #29484 with ECRH injection on the $q = 2$ surface.

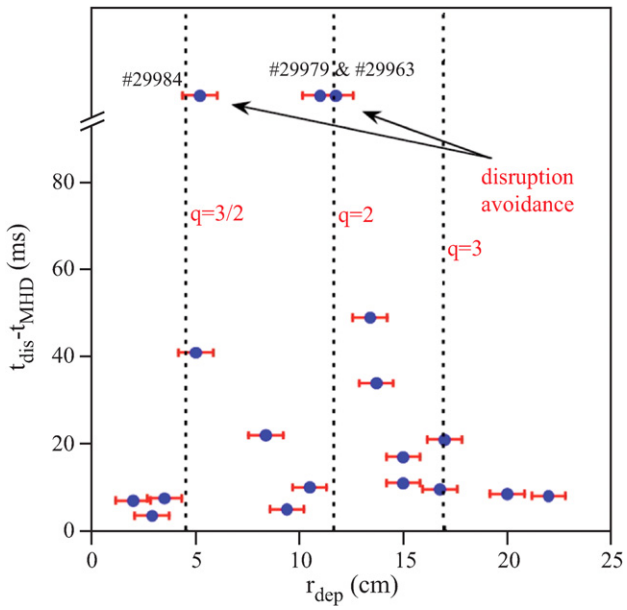

Figure 9. FTU power deposition scan: current quench delay versus r_{dep}; t_{dis} = time of current quench; t_{MHD} = time of abrupt rise of MHD activity. The vertical axis is interrupted above 80 ms to accommodate discharges with disruption avoidance.

envisaged in order to suppress islands that are not directly heated by ECRH waves. In density limit disruptions, when ECRH cannot be absorbed on the central 3/2 mode due the density cut-off, avoidance might be obtained by heating a more external coupled island where the density is below cut-off. In other cases, P_{ECRH} might be deposited on the coupled island that requires less power for stabilization.

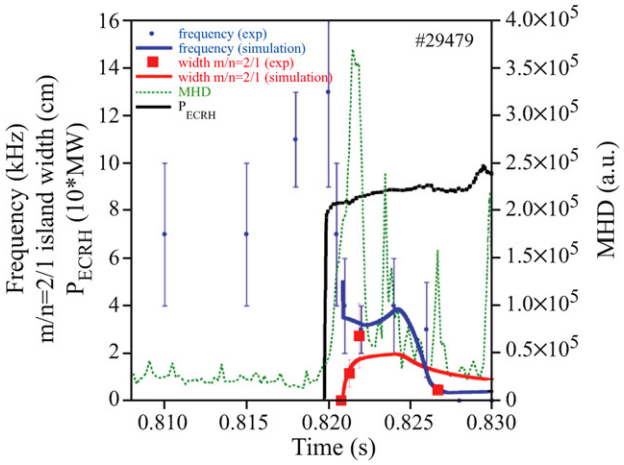

Figure 10. Time evolution of 2/1 mode, close to mode locking time, compared with the Rutherford model. Experimental frequency from Mirnov coils, MHD represents the B_θ oscillations envelope and island width is determined from soft x-ray tomography.

5. Investigating dust dynamics in tokamak plasma

Since 2005, research activity on dust in fusion plasma has been pursued on FTU in collaboration with the Max Planck Institute for Extraterrestrial Physics (MPE) of Garching, the Royal Institute of Technology (KTH) of Stockholm and the Universities of Naples and Molise. Theoretical issues on dusty plasma physics [34, 35] have been addressed and experiments have been performed on FTU [36–38]. The detection, in the FTU SOL, of micron size fast dust particles, impinging on PFCs at velocity of the order of 10 km s^{-1}, has been already reported [36]. Such particles produced uncorrelated spikes in the ion saturation current signal detected by two adjacent Langmuir probes. Interpretation of these events in terms of the dust impact ionization events was supported by the SEM observation of typical impact craters on the probe surface. A more accurate analysis [37] has shown that the impact ionization events can be identified by suitable choice of the threshold amplitude of the observed spikes. The number of impact events detected matches reasonably the number of craters observed. Analyses of the features of the spiky signals, as well of the morphology of the craters observed, see figure 11, suggests the exclusion of possible alternative interpretations. To this end, an experimental campaign was planned to collect and analyse fast grains by silica aerogel targets [39]. This highly porous, very low density material allows capture of the fast dust particles without affecting them, and might provide information on the velocity and size distribution as well as on the dust composition. A preliminary assessment of the compatibility of silica aerogel targets with the FTU vacuum and plasma operation was carried out. The mechanical design and construction of the sample holder has been done and the sample introduction system has been improved to allow the aerogel experiments in the next campaign. The feasibility of this new method of dust collection has been suggested by preliminary tests on the HT-7 [40] and in the reversed field-pinch EXTRAP-T2R [40]. A design has been undertaken of an electro optical probe to detect the emission of light associated with a dust impact ionization event and simultaneously record the perturbation (spike) it will produce on the ion saturation

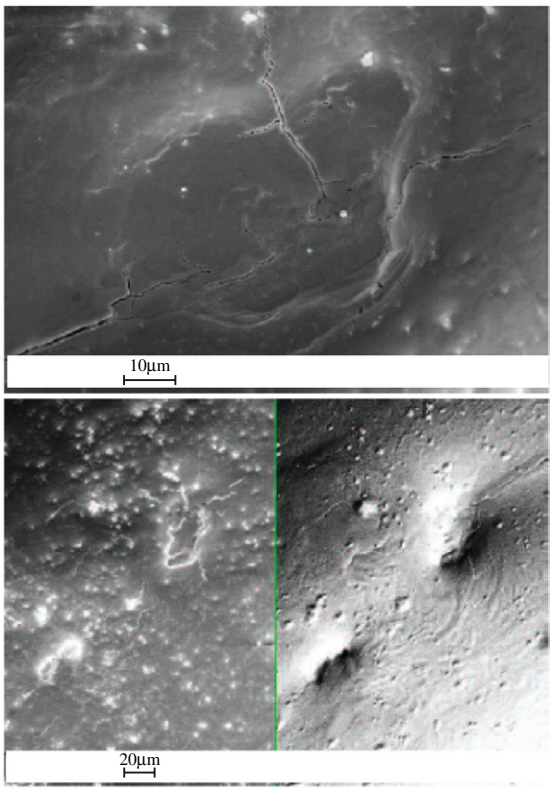

Figure 11. SEM analysis of the probe surface exposed to the FTU plasma. The scales indicated are 10 μm in the upper figure, taken by secondary electron detector (SED) and 20 μm for the lower figure, where SED (left) and electron back scattering (EBS) (right) images are compared for the same probe area.

current. Impact ionization events can be discriminated from interaction of plasma structures, generally characterized by large ($\gg$1 cm) correlation length in toroidal direction, utilizing two spherical probe tips of 2 mm diameter, located 1 cm apart in the toroidal direction. The photon yield due to the impact of 1 μm iron grain impinging at 10 km s^{-1} on a probe tip made of tungsten (an element which is not contained in PFCs of FTU), has been evaluated assuming a 1 mm diameter optical fibre collector located at a distance of 1 cm from the light source. Preliminary results suggest that a few thousands photons, emitted in the main line of the W neutrals vaporized upon impact, can be detected during the interval of a few tens of microseconds of light emission following the impact. The modelling of the light emission process is consistent with the light emission observed upon hypervelocity dust impacts [41].

A characterization of the molybdenum (main limiter material in FTU) dust component present in the FTU vacuum chamber has been attempted by laser light elastic scattering [38]. The detection channels at the laser wavelength (λ = 1064 nm) of the Thomson scattering diagnostic were used. The signal was detected on many discharges after disruption. No evidence of scattering by dust was found indeed in the main plasma during normal operations, nor was it possible to look at the SOL as no channels are aiming there. The particle size was estimated from the intensity of the scattered light, with Rayleigh modelling of the laser-dust elastic cross section. This approximation seems reasonable for particles with size less than 0.1 μm (about 10% λ); however, the diagnostics becomes

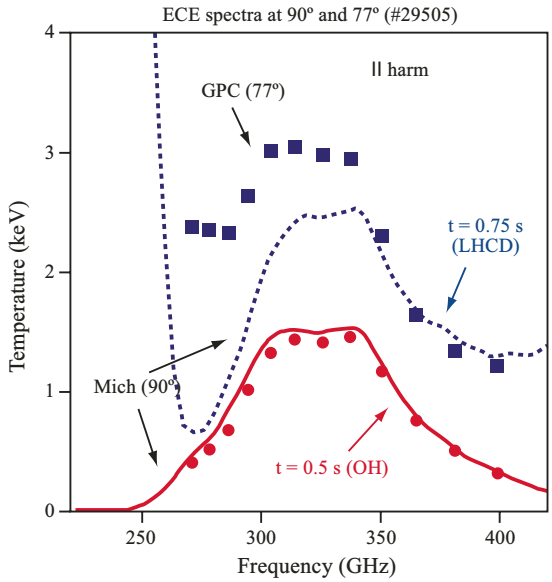

Figure 12. ECE emission at 90° (continuous and dotted lines) and 77° (dots and boxes) in OH (continuous line and dots) and LHCD (dotted line and boxes) phase.

very insensitive to particles smaller than a few tens nanometres. Assuming typical values of the refractive index expected for molybdenum dust grains, the average radius of the dust grains detected after disruption was found of the order of 50 nm. Recent improvement of the sizing, obtained by the Thomson scattering diagnostic, on the dust produced upon disruptions of FTU discharges, taking into account the Mie theory and the effects of laser light particle evaporation, suggests that the Rayleigh scattering approximation underestimates the particle diameters by a factor 2–5. The average dust density was found about $10^7\ m^{-3}$, calculated as the total number of scattering events, divided by the product of the scattering volume and the total number of the laser pulses considered. The size distribution of the particles seems to follow a power law s^{-2}, where s is the geometrical cross section of the grains [10].

6. Minor upgrades and future plans

Since the last FEC a long-term programme of upgrading has been undertaken on FTU. The main objective is the refurbishment of the heating systems, to have the full power reinstated, together with the realization of a new launching structure for ECRH. This structure will be steerable in real time, will allow a CTS experiment in an ITER-relevant configuration and will allow injection at a large off-normal angle. In particular this latter capability will be used to operate in mode conversion thus enabling heating high density peaked plasmas above the 140 GHz cut-off density. Minor diagnostics upgrades have already been completed and have initiated the commissioning on FTU: oblique ECE, refractometer and MSE. The MSE commissioning has been slowed down due to hardware rearrangement needed to optimize detection and signal to noise ratio. This has been an acceptable limitation as in parallel the experimentation on advanced scenarios has been delayed by the RF power refurbishment.

A prototype of a time-of-flight refractometer at 60 GHz, has been tested in FTU, in collaboration with TRINITI institute (Moscow). Line density measurements are in good agreement with those measured with a CO_2 interferometer. This system has reduced size, does not require mirrors inside the vessel and is not affected by fringe jumps: therefore it seems to be a good candidate for the ITER density feedback control. A system with two frequencies is under development.

The antenna of the ECE grating polychromator (GPC) has been modified to steer its lines of sight in the toroidal direction from 90° to 72°. EC emission at different angles comes from different regions of the electron distribution function, providing a diagnostic of possible distortions of the maxwellian. The information can be reconstructed using an emission code where the distribution function is the trial function. Preliminary results have been obtained during LHCD, where a supra-thermal electron tail is driven, and during a strong central ECRH at low density, where the bulk of the distribution is directly affected. During LHCD, at intermediate density ($\sim 9 \times 10^{19}\ m^{-3}$), the second harmonic X-mode emission at 77° is higher than that measured at 90° by the Michelson interferometer (see figure 12), as expected for the contribution of the up shifted emission that is not reabsorbed by the thermal electrons. The difference between the two emissions is an indication of the number of the 'up shifted electrons' and their energy. The data interpretation, however, is much more complex considering that (a) supra-thermal emission is not radially localized, (b) at higher frequencies (above 350 GHz) the third harmonic down shifted emission overlaps the second harmonic, (c) the O-mode contribution, for oblique view, is not negligible. Measurements during strong ECRH heating, in the current ramp-up, are even more difficult to reconstruct as the distortion of the distributions can only be obtained by a Fokker–Plank code. The only clear effect on the emission is a stronger decrease with the observation angle respect to that of thermal plasmas. The distortion found in previous works [42, 43] is an asymmetric flattening of the distribution function at the resonance.

7. Conclusions

The synergy between theory and experiment has been key to the relevance of the FTU results. Experimental activity on FTU addresses physics and technological issues extremely relevant on the path towards the realization of fusion reactors. Encouraging results are being obtained testing a LLL as a possible solution for handling the high heat loads already expected in ITER. Meanwhile, conditions associated with lithized walls have produced a new high density regime characterized by peaked profiles. ECRH localized heating above cut-off will be necessary to probe the transport characteristics of this regime. The realization of the new ECRH launcher will allow this scenario via electron Bernstein wave conversion. Burning plasma physics is addressed through the study of the fishbone instabilities triggered by the LH generated fast electrons. Important confirmations are already obtained; while a complete benchmarking between theory and experiments is progressing through a systematic exploration of the plasma parameter space and waves power scan. New theoretical and experimental results are obtained in the area of beta induced Alfven eigenmodes where new gaps have been

found in the SAW continuous spectrum when magnetic islands are present. Further experiments will confirm the feasibility of utilizing magnetic island induced Alfvén eignemodes continuum effects as a novel magnetic island diagnostic based on the dependence of the frequency on the magnetic island size. Finally FTU results have made an important contribution in the field of plasma stability control. The use of ECRH to stabilize MHD modes and to avoid disruptions has been assessed providing an interesting alternative to massive gas injection as a tool for avoiding disruptions in the reactor.

8. References

[1] Gormezano C. ed 2004 *Fusion Sci. Technol.* **45** 357–401 and 459–82 (Special issue on FTU)

[2] Zonca F. *et al* 2007 Electron fishbones: theory and experimental evidence *Nucl. Fusion* **47** 1588

[3] Cesario R. *et al* 2008 Fishbone-like instability driven by LH generated fast electrons on FTU *Proc. 22nd Int. Conf. on Fusion Energy 2008 (Geneva, Switzerland, October 2008)* (Vienna: IAEA) file EX-P8-12 http://www-naweb.iaea.org/napc/physics/FEC/FEC2008/html/index.htm 2009 *Nucl. Fusion* submitted

[4] Mazzitelli G. *et al* 2008 Status and perspectives of the liquid material experiments in FTU and ISTTOK *Proc. 22nd Int. Conf. on Fusion Energy 2008 (Geneva, Switzerland, October 2008)* (Vienna: IAEA) file EX-P4-6 http://www-naweb.iaea.org/napc/physics/FEC/FEC2008/html/index.htm

[5] Esposito B. *et al* 2008 Disruption control on FTU with ECRH *Proc. 22nd Int. Conf. on Fusion Energy 2008 (Geneva, Switzerland, October 2008)* (Vienna: IAEA) file EX/7-3Ra, http://www-naweb.iaea.org/napc/physics/FEC/FEC2008/html/index.htm 2009 *Nucl. Fusion* **49** 065014

[6] Buratti P. *et al* 2005 *Nucl. Fusion* **45** 1446

[7] Annibaldi S.V. *et al* 2007 *Plasma Phys. Control. Fusion* **49** 475

[8] Zimmermann O. *et al* 2005 Coupling of Alfvén-like modes and large 2/1 tearing modes at TEXTOR *Proc. 32nd EPS Conf. on Plasma Phys. Control. Fusion (Tarragona, Spain, June 2005)* vol 29C (ECA) P-4.059 http://epsppd.epfl.ch/Tarragona/pdf/P4_059.pdf

[9] Biancalani A. *et al* 2008 Shear Alfvén wave continuous spectrum in the presence of a magnetic island *Proc. 22nd Int. Conf. on Fusion Energy 2008 (Geneva, Switzerland, October 2008)* (Vienna: IAEA) file TH/P3-5 http://www-naweb.iaea.org/napc/physics/FEC/FEC2008/html/index.htm

[10] Castaldo C. *et al* 2008 Dust detection in FTU *Proc. 22nd Int. Conf. on Fusion Energy 2008 (Geneva, Switzerland, October 2008)* (Vienna: IAEA) file EX/P4-5 http://www-naweb.iaea.org/napc/physics/FEC/FEC2008/html/index.htm

[11] Apicella M.L. *et al* 2007 *J. Nucl. Mater.* **363–365** 1346

[12] Evtikhin V.A. *et al* 2001 *Fusion Eng. Des.* **56–57** 363

[13] Mazzitelli G. *et al* 2007 Experiments on FTU with a liquid lithium limiter *Proc. 34th EPS Conference on Plasma Phys. (Warsaw, Poland, July 2007)* ed P. Gasior and J. Wolowski vol 31F (ECA) O-2.001 http://epsppd.epfl.ch/Warsaw/pdf/O2_001.pdf

[14] Pericoli-Ridolfini V. *et al* 2007 *Plasma Phys. Control. Fusion* **49** S123

[15] Esposito B. *et al* 2004 *Plasma Phys. Control. Fusion.* **46** 1793

[16] Cenacchi G. and Taroni A. 1986 The JET equilibrium-transport code for free boundary plasmas *Proc. 8th Europhysics Conf. on Computational Physics, Computing in Plasma Physics (Eibsee, Germany, 1986)* vol 10D (EPS) p 57

[17] Romanelli M. *et al* 2006 *Nucl. Fusion.* **46** 412

[18] Pericoli-Ridolfini V. *et al* 2007 *Nucl. Fusion* **47** S608

[19] Wong K.L. *et al* 2000 *Phys. Rev. Lett.* **85** 996

[20] Macor A. *et al* 2008 Fast particle triggered modes: experimental investigation of electron fishbones on TORE SUPRA *Proc. 35th EPS Conf. on Plasma Phys. (Hersonissos, Crete, Greece, June 2008)* P-4.062 http://epsppd.epfl.ch/Hersonissos/pdf/P4_062.pdf

[21] Cesario R. *et al* 2004 *Phys. Rev. Lett.* **92** 175002

[22] Smeulders P. *Tomography on Lao-Hirschman type of equilibria using mode rotation Proc. 34th EPS Conf. on Plasma Phys. (Warsaw, Poland, July 2007)* ed P. Gasior and J. Wolowski vol 31F (ECA) P-5.069 http://epsppd.epfl.ch/Warsaw/pdf/P5_069.pdf

[23] Gomez P. *et al* 2001 *Fusion Eng. Des.* **53** 169

[24] Chen L. and Hasegawa A. 1974 *Phys. Fluids* **17** 1399

[25] Kieras C.E. and Tataronis J.A. 1982 *J. Plasma Phys.* **28** 395

[26] Furth H.P. *et al* 1963 *Phys. Fluids* **6** 459

[27] Biancalani A. *et al* Continuous spectrum of shear Alfvén waves in the presence of a magnetic island *Proc. 35th EPS Conf. on Plasma Phys. (Hersonissos, Crete, Greece, June 2008)* http://epsppd.epfl.ch/Hersonissos/pdf/P1_051.pdf

[28] Chu M.S. *et al* 1992 *Phys. Fluids* B **4** 3713

[29] Riccardo V. and Loarte A. 2005 *Nucl. Fusion* **45** 1427

[30] Esposito B. *et al* 2008 *Phys. Rev. Lett.* **100** 045006

[31] Zohm H. *et al* 1995 *Plasma Phys. Control. Fusion* **37** A313

[32] Nowak S. and Orefice A. 1994 *Phys. Plasmas* **1** 1242

[33] Ramponi G. *et al* 1994 *Phys. Plasmas* **6** 3561

[34] Castaldo C. *et al* 2006 *Phys. Rev. Lett.* **96** 075004

[35] De Angelis U. *et al* 2006 *Plasma Phys. Control. Fusion* **48** B91

[36] Castaldo C. *et al* 2007 *Nucl. Fusion* **47** L5

[37] Ratynskaia S. *et al* 2008 *Nucl. Fusion* **48** 015006

[38] Giovannozzi E. *et al* 2007 Dust measurement with Thomson scattering in FTU *Burning Plasma Diagnostics International Conf. (Varenna, Italy, 24–28 September 2007) AIP Conf. Proc.* **988** 148

[39] Tsou P. 1995 *J. Non-Crys. Solids* **186** 415

[40] Ratynskaia S. *private communication*

[41] Eichorn G. *et al* 1976 *Planet. Space Sci.* **24** 771

[42] Tudisco O. *et al* 2001 Oblique ECE Measurements during Strong ECH at 140 GHz in FTU *Proc. 28th EPS Conf. on Controlled Fusion and Plasma Physics (Funchal, 2001)* vol 25A 1221 P3.082 http://epsppd.epfl.ch/Madeira/html/pdf/P3.082.pdf

[43] Krivenski V. 2001 *Fusion Eng. Des.* **53** 23